Shi et al. *NPG Asia Materials* (2022) 14:47
https://doi.org/10.1038/s41427-022-00391-7

NPG Asia Materials

ARTICLE Open Access

Vapor phase polymerization of Ag QD-embedded PEDOT film with enhanced thermoelectric and antibacterial properties

Wei Shi[1,2], Qin Yao[1], Wang Donghui[3], Sanyin Qu[1], Yanling Chen[1], Kyu Hyoung Lee[2] and Lidong Chen[1]

Abstract

Nonferric oxidant precursors have the unique advantage of directly polymerizing poly(3,4-ethylenedioxythiophene) (PEDOT)-inorganic composites. However, due to limited solubility and unmatched oxidation potentials, most oxidants only produce powders or porous materials. To obtain high-quality films with improved homogeneity and controllable particle sizes, the oxidants should be adaptable to high-standard PEDOT film fabrication techniques such as vapor phase polymerization (VPP). In this work, we discovered for the first time a nonferric metal salt suitable for the VPP process. With the addition of an Fe(III) salt to stabilize the reaction and adjust the oxidant ratio, micron-thick antibacterial S-PEDOT-Ag quantum dot (QD) composite films with tunable Ag wt% can be synthesized in one facile step. With a low Ag loading of ~0.2 wt%, the film exhibited an optimized power factor of 63.1 μW/mK^2, which is among the highest values thus far reported for PEDOT-metal composites. Increase of the Ag(I) concentration in the precursor to a certain level may lead to minor decomposition of the polymer followed by the formation of Ag_2S particles.

Introduction

Conducting polymer (CP)-based nanocomposites have received extensive attention for various applications, such as in thermoelectrics (TE)[1], photovoltaics[2], supercapacitors[3], and sensors[4]. Poly(3,4-ethylenedioxythiophene) (PEDOT) is among the most widely studied systems because of its good electrical properties and chemical stability. When synthesizing PEDOT-based nanocomposites, the commercially available, water-soluble PEDOT:polystyrenesulfonate (PEDOT:PSS) is most often used. When doped with a hydrophilic polyanion, the PEDOT:PSS aqueous solution provides a convenient approach to produce various composites through simple solution processes. In the TE field, there are numerous reports on syntheses of PEDOT:PSS/inorganic composites using various inorganic components, such as 2D carbon materials, tellurium-based materials and metal particles[5,6]. However, the water processability of PEDOT:PSS comes at the cost of electrical properties. The presence of large polyanions and undoped excess sulfonate groups results in amorphous structures and decreased transport properties[7,8]. The concentration of PEDOT:PSS in aqueous solution is difficult to increase (usually less than 1 wt%), which tends to cause sedimentation of inorganic particles. Furthermore, direct mixing or in-situ reactions often cause oxidation of nanoparticles (NPs)[9,10] or reduction of polymers[11].

Recently, small-sized anion doped PEDOT (S-PEDOT) has come into view as a potential base material for next-generation CP-inorganic nanocomposites. Without excess undoped segment, S-PEDOT exhibits compact and crystallized structure that enables good electrical performance[8,12,13]. It is not difficult to acquire S-PEDOT with σ above 1000 S/cm through variously reported approaches[12,14–16] or to

Correspondence: Qin Yao (yaoqin@mail.sic.ac.cn) or Kyu Hyoung Lee (khlee2018@yonsei.ac.kr) or Lidong Chen (cld@mail.sic.ac.cn)
[1]State Key Laboratory of High Performance Ceramics and Superfine Microstructure, Shanghai Institute of Ceramics, Chinese Academy of Sciences, Shanghai, China
[2]Department of Materials Science and Engineering, Yonsei University, Seoul, South Korea
Full list of author information is available at the end of the article

further optimize the performance through dedoping or anion substitution[17–20]. However, there are still large challenges, especially in precise control of the synthetic process to obtain high-performance polymers. Electrical performance is very sensitive to fabrication parameters such as basicity[21], humidity[15,22], temperature[23], film thickness[24], surfactants[25,26], and dopants[27–29]. Furthermore, high-performance S-PEDOT films can only be synthesized via nonsolution processes, such as solution casting and vapor phase polymerization (VPP), which require highly concentrated oxidant solution with sufficient viscosity for spin-coating. The film is completely insoluble after the initial synthesis. It is therefore even more challenging to produce S-PEDOT-based composites with controllable microstructures and doping levels.

In our previous work, we developed a single component inhibitor-free oxidative solution that realized self-inhibited polymerization and allowed easy-to-control fabrication of micron-thick S-PEDOT films through the VPP approach[28]. Thereafter, a one-step synthesis of a S-PEDOT-Te quantum dot (QD) composite film was realized by introducing the secondary nonferric oxidant $TeCl_4$[30]. The film exhibited a maximum power factor above 100 μW/mK^2. Unlike conventional ferric salt oxidants that only induce polymerization (1), multifunctional nonferric oxidants allow the simultaneous formation of polymer and inorganic NPs (2). The nanosized particles enveloped in the hydrophobic S-PEDOT matrix are protected from oxidation, particle loss, and agglomeration.

$$Fe^{3+} + \mathrm{A}^- + \mathrm{EDOT} = \mathrm{PEDOT:A} + Fe^{2+} + \mathrm{HA} \quad (1)$$

$$M^{x+} + \mathrm{A}^- + \mathrm{EDOT} = \mathrm{PEDOT:A} + M^0 + \mathrm{HA} \quad (2)$$

To extend the abovementioned work to more material systems, we took notice of previously reported nonferric precursors, most of which were metal salts, including $Ce(SO_4)_2$[31], $AgNO_3$[32], $Cu(NO_3)_2$[32], $HAuCl_4$[33], and $CuCl_2$[34–36]. In these reports, PEDOT-based composites were often synthesized through solution processes or CVD. However, owing to the low solubilities and unmatched oxidation potentials of these oxidants, polymerizations are uncontrollable and often must be carried out in diluted solution. Only powder-like or porous composites could be obtained. The unsatisfactory structures limited the electrical performance of the composites. If we can improve the solubility of these metal salts and control their oxidability, syntheses of high-performance new composites through standard VPP or solution casting processes are expected for exploring various applications.

In the present work, we realized for the first time a one-step synthesis of a micron-thick nonporous PEDOT-metal composite film through VPP by using a multifunctional metal salt oxidant. The obtained PEDOT-Ag QD composite films exhibited enhanced TE performance and antibacterial effects at low Ag concentrations of ~ 0.2 wt%. The formation of Ag_2S QDs caused by partial decomposition of the polymer was observed at higher Ag(I)/Fe(III) precursor ratios. This research provides an effective route to introduce homogeneous metal QDs in the CP matrix as well as some universal strategies for syntheses of high-performance conducting polymer composites.

Experimental procedures

Preparation of the oxidative solution

The synthesis of $FeDBSA_3$ was based on previously described procedures[28]. Sodium dodecylbenzenesulfonate (SDS, 66.0278 g, 95%, Aladdin, China) was dissolved in 600 mL of deionized water and the solution was heated to 60 °C. Bubbles were eliminated by blowing the surface with dry air. Then, 24.5724 g of iron chloride hexahydrate ($FeCl_3{\cdot}6H_2O$, 99%, Sinopharm, China) was dissolved in 75 mL of deionized water to make an $FeCl_3$ solution. Thereafter, the $FeCl_3$ solution (excess amount) was quickly dripped into the hot SDS solution with stirring. The precipitate was washed with deionized water 10 times. Then, it was dissolved in ethanol and evaporated in a rotary evaporator at 130 °C. To prepare AgDBSA, 10.3102 g of dodecylbenzensulfonic acid (DBSAH, 95%, Aladdin) was dissolved in 50 mL of ethanol. A few drops of water were added to increase the acidity. Then, 5 g of silver carbonate (Ag_2CO_3, 99%, Aladdin) was added to the solution. The mixture was stirred for 48 h. After removing the insoluble material by centrifugation, the clear solution was evaporated in a rotary evaporator at 95 °C. Afterward, $FeDBSA_3$ and AgDBSA were separately dissolved in a certain amount of ethanol and mixed at the desired ratio. Finally, each solution was concentrated to a concentration of approximately 75 wt% by repeating the evaporation and dissolving processes.

Syntheses of nanocomposite films

The oxidative solution was spin-casted at 2000–6000 rpm for 30 s onto 18 × 18 mm glass substrates. Then, the coated substrates were preheated on a hot plate at 90 °C for 60 s and exposed to EDOT monomer in a quartz reaction chamber filled with EDOT monomer heated to 90 °C. The reaction time was 10–25 min depending on the Ag(I) concentration. After the reaction, the samples were immediately washed with ethanol and then dried at ambient temperature.

Characterization

Film resistance was measured by the Van der Pauw method using a Hall measurement system (HL5500PC). Film thickness was measured by a profilometer (DEKTAK-XT). Scanning electron microscopy (SEM, Verios

G4 UC) and atomic force microscopy (AFM, NTEGRA MT-MDT) were used to observe the inner and surface morphologies of the composite films. An energy-dispersive spectrometer (EDS) was used to measure the Ag concentration in the PEDOT film. A high-resolution transmission electron microscope (HRTEM, Tecnai G2 F20) was used to determine the particle sizes and phases of the NPs. Grazing incidence X-ray diffraction (GIXRD, Rigaku D/max 2550 V) and Raman spectra (Renishaw InVia) were used to determine the crystal structures and chemical structures of the materials. The doping level and S/Ag ratio were determined by X-ray photoelectron spectroscopy (ESCAlab 250). The temperature dependence of conductivity, carrier concentration, and carrier mobility were determined with a physical property measurement system (PPMS-9, Quantum Design). The Seebeck coefficients were measured with a homemade device with a polyimide heating film and two R-type thermocouples monitoring both the temperature difference and Seebeck voltage. The antibacterial activity of the composite film was examined with the live/dead staining and bacterial counting method using *Escherichia coli* (*E. coli*, ATCC 25922). *E. coli* cells were cultured in Luria–Bertani (LB, Sigma, USA) broth or LB agar plates. All samples were sterilized with 75% ethanol solution and placed in a 24-well bacterial culture plate before bacterial culture. Then, 60 μL of bacterial solutions with concentrations of 10^7 CFU/mL were dripped onto the sample surface and incubated in a 37 °C incubator for 24 h. *E. coli* cultured on various samples were stained by the Live/Dead Baclight™ Bacterial Viability Kits (L13152, BioVision). A laser scanning confocal microscope (LSCM, SP8, Leica) was used to observe the distributions of live/dead bacteria on the surfaces of the samples. ^{1}H nuclear magnetic resonance (^{1}H-NMR, Avance III HD 300) and liquid chromatography–mass spectrometry (LC–MS, Ultimate 3000 RS-Q-Exactive Orbitrap Plus) were used to analyze the side reactions caused by Ag(I).

Results and discussion

With moderate oxidation potentials ($E(Ag^+/Ag) = 0.80$ V vs. SHE) close to that of Fe(III) ($E(Fe^{3+}/Fe^{2+}) = 0.77$ V vs. SHE), Ag salts are theoretically ideal oxidants for polymerizing S-PEDOT. Compared with some other Ag salt candidates (such as those with trifluoromethanesulfonate, tosylate, camphorsulfonate, and methanesulfonate), silver dodecylbenzenesulfonate (AgDBSA) exhibits significantly higher solubility owing to the large surfactant anion, which enabled preparation of ethanol solutions with > 70 wt% solute for spin-coating. We initially performed a VPP synthesis using pure AgDBSA. The reaction proceeded very rapidly, and the precursor layer reacted almost instantly when exposed to the EDOT monomer. A possible explanation for this is that Ag(I) salts are almost 3 times smaller in size than Fe(III) salts. The smaller size increases the effective concentration of the oxidant when the solvent is evaporated during polymerization. Furthermore, Ag(I) is also much less coordinated by solvent molecules than Fe (III), which leads to a higher oxidation potential. The poorly polymerized sample disintegrated during the washing process. To solve this problem, we added an additional Fe(III) oxidant ($FeDBSA_3$) with a self-inhibiting function, as developed in our previous work[28], the reaction rate was effectively reduced without using inhibitors. The high solubility of $FeDBSA_3$ also enabled a higher solution viscosity, which allowed the film thickness to exceed 3 μm. Furthermore, the Ag concentration was conveniently adjusted by changing the Ag(I)/Fe(III) ratio. Table 1 shows the Ag wt% expected for the corresponding Ag(I)/Fe(III) ratio, and Scheme 1 illustrates the synthetic process.

SEM (back-scattered) images and HRTEM images of the nanocomposite film are shown in Fig. 1. The corresponding secondary electron images are shown in Fig. S1. The film is nonporous, with Ag NPs homogeneously dispersed in the polymer matrix. The Ag concentrations acquired from EDS (Fig. S2, modified according to the XPS results) agreed well with the theoretical values shown in Table 1, indicating that all Ag(I) precursors reacted completely with EDOT monomers. When Ag concentrations were below 5 wt% (P1–P4), Ag particle sizes were mostly <5 nm (QD-scale) and exhibited cubic structure (Fig. 1b). At higher Ag concentrations (P5-P10), the Ag-containing particles mostly exhibited the monoclinic Ag_2S phase (Fig. 1c). The remaining TEM data are shown in Fig. S3. According to the XPS results (discussed in the next section), there was actually an intermediate area between P4 and P5 in which both phases existed. The sizes of Ag-containing particles did not increase much at higher Ag(I) precursor ratios, since the formation of Ag_2S might have hindered the growth or merging of Ag crystals.

Table 1 Ag(I)/Fe(III) ratio and the calculated weight percentage of samples.

Sample No.	P0	P1	P2	P3	P4	P5	P6	P7	P8	P9
Ag(I)/Fe(III)	0	0.0025	0.005	0.01	0.025	0.05	0.1	0.3	0.5	1.0
Ag wt%[a]	0	0.2	0.5	1.0	2.3	4.4	8.1	18.7	24.7	34.0

[a]The results are modified using the exact doping levels according to the XPS results. The formation of Ag2S is also taken into account, which has only slight influence on the overall data.

Ag 3d and S 2p XPS spectra (Fig. 2a) were used to determine the doping levels[15] as well as the Ag/Ag_2S ratios. After calibrating the data with the maximum thiophene S 2p signal at 163.65 eV, six different S 2p signal peaks were identified. The doublets at 170–165.5 eV (blue), 167–162.5 eV (green) and 163.1–160.1 eV (olive) belonged to the $DBSA^-$ counterion, thiophene ring and Ag_2S, respectively. The intensity of the Ag 3d signal (366–376 eV) increased with increasing Ag concentration. It is difficult to determine the oxidation status directly from the Ag 3d signal because the peak shift between the two oxidation states is less than 0.5 eV (details are discussed in the Supporting Information, Fig. S4). However, we can still calculate the S^{2-}/Ag ratio (Fig. 2b) by comparing the strength-modified integrated area ratio of the S 2p/Ag 3d signal. The signal strength factors for S 2p and Ag 3d were 22.13 and 1.88, respectively. The results showed that the particles almost completely consisted of elemental Ag when the particle concentrations were below 1.0 wt% ($S^{2-}/Ag = 0$). At higher Ag wt%, Ag_2S formation gradually dominated. Almost all particles within the film were transformed into Ag_2S when the Ag wt% was higher than 8.1 wt% (P6-P9, $S^{2-}/Ag = 0.5$). The doping level (also displayed in the same figure) was calculated from the ratio of integrated areas for the counterion and thiophene signals ($r^2 > 0.996$), which decreased with increasing Ag(I)/Fe(III) ratio. The doping ability was nearly halved at higher oxidant ratios, which indicated a lower degree of polymerization caused by a high reaction rate or damaged end-groups. At high Ag(I)/Fe(III) ratios, a special odor can be distinguished during the reaction, which probably comes from a product of decomposition. ^{1}H-NMR (Fig. S5) and LC–MS (Fig. S6) results indicated that a high Ag^+ concentration resulted in disconnection of the C–S bond in the end group, which stopped chain growth and resulted in the formation of Ag_2S.

Raman spectra (Fig. 2c) were used to further analyze changes in the structure of the polymer. The overall data and a peak table are available in Fig. S7. The spectra were normalized by taking the peaks at 439, 578, and 990 cm^{-1} (blue, representing oxyethylene ring deformations) as reference peaks. Multiple additional peaks (marked with dark red triangles) were observed at high Ag(I) precursor concentrations. These peaks are believed to originate from the abovementioned decomposition of thiophene units at high Ag(I) ratios. There were also significant

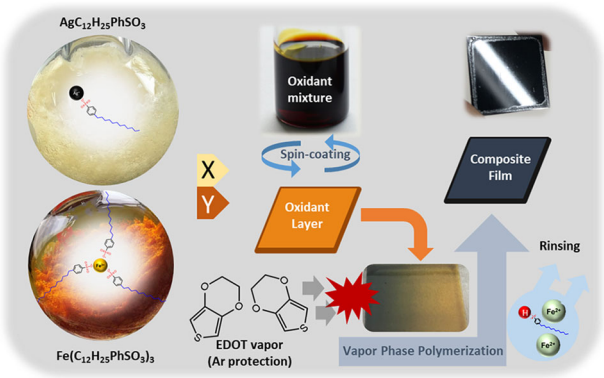

Scheme 1 Self-inhibited polymerization of the composite film using Ag(I)/Fe(III) oxidant.

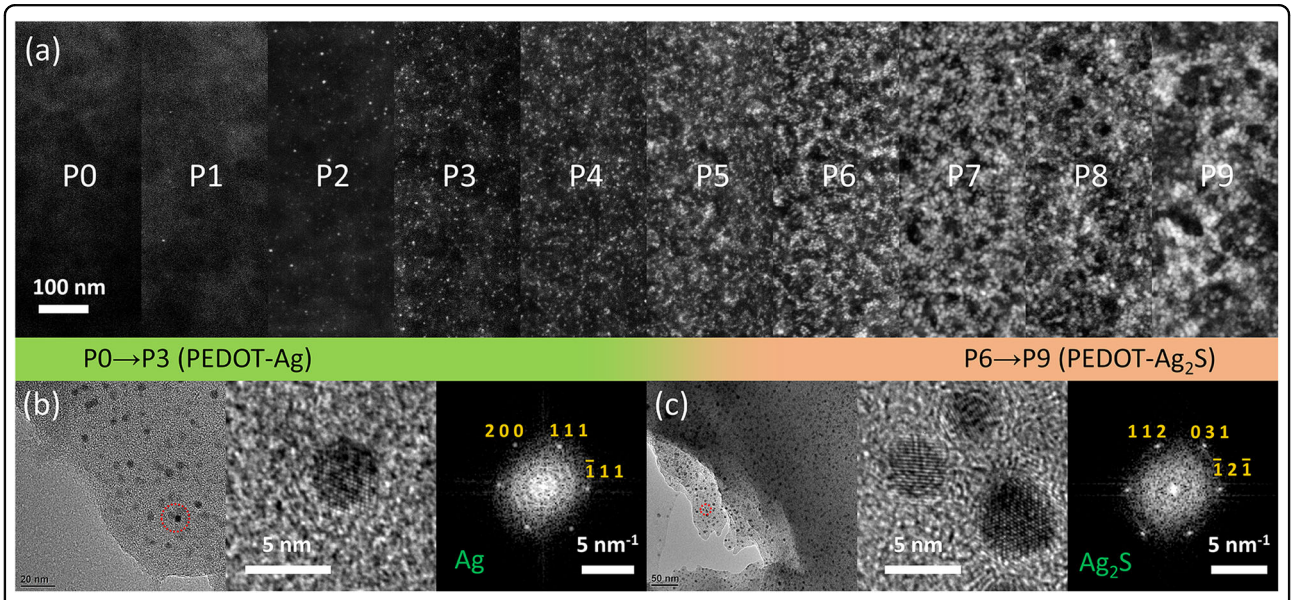

Fig. 1 Microscopic images of pristine/composite films. a SEM (back-scattered) images of samples P0-P9; **b** HRTEM images and diffraction patterns of sample P4; **c** HRTEM images and diffraction patterns of sample P6.

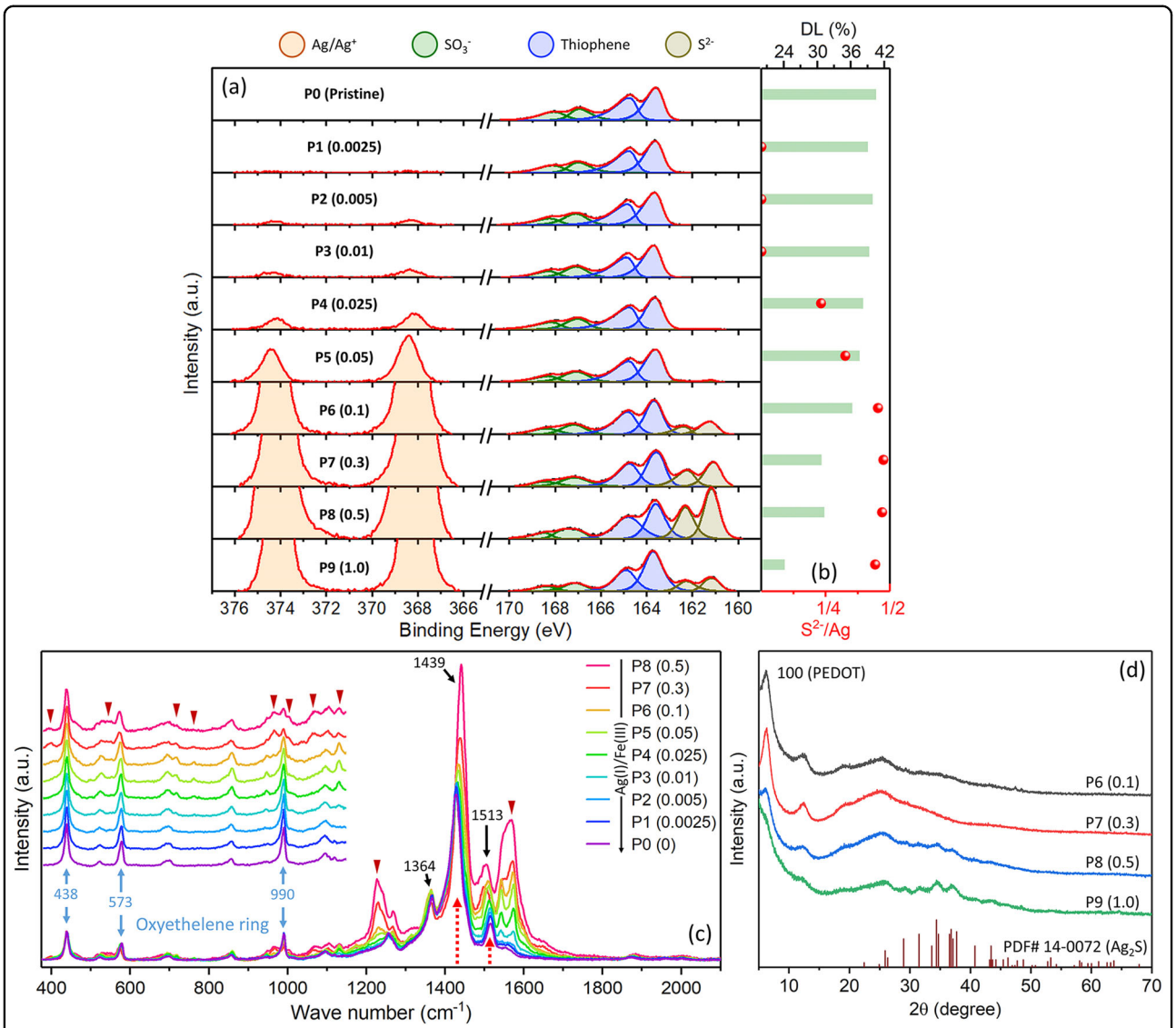

Fig. 2 Structural characterizations. a Ag 3d (left) and S 2p (right) XPS spectra of PEDOT-Ag/Ag_2S nanocomposite films. The doublets at 170–165.5 eV (blue), 167–162.5 eV (green), 163.1–160.1 (olive), 366–376 eV (orange) are from the sulfonate counter ion, thiophene chain, S^{2-} and Ag, respectively. **b** Doping level (DL) acquired from the integrated area ratio of the counterion (blue) and thiophene signals (green), and S^{2-}/Ag ratio determined by the integrated area ratio of the corresponding signal peaks (olive and orange). **c** Raman spectra of nanocomposite films. **d** GIXRD image of PEDOT-Ag_2S nanocomposite films. Angle of incidence: 0.4°. Scan speed: 0.5°/min.

increases in benzoid absorbances at 1428 and 1517 cm^{-1} with increasing Ag(I)/Fe(III) ratios, which indicated a decrease in quinoid structures as well as conjugation between thiophene rings. The GIXRD results (Fig. 2d) also showed a decrease in the PEDOT (100) peak signal intensity due to structural disordering.

The quality of the PEDOT matrix is essential for the protection of NPs. Strong self-shrinkage of the polymer during the drying process[5] ensured a high film density and low surface roughness of the film. However, this effect was diminished at high Ag(I) oxidant ratios because a low degree of polymerization and partial decomposition of the polymer weakened the interactions between polymer chains. With an increasing number of particles remaining within the increasingly fragile polymer matrix, the surface roughness of the film increased drastically. The AFM results (Fig. 3a, b) showed that the surface roughness (R_q) increased drastically when the Ag(I)/Fe(III) ratio exceeded 0.1. The loose polymer matrix resulted in particle loss during the washing process, causing the actual Ag wt% to be lower than the calculated value (Fig. S2). The color of the film gradually changed with increasing particle concentration (Fig. 3c).

The composite films exhibited lower electrical conductivities (σ) and carrier concentrations (n) than the

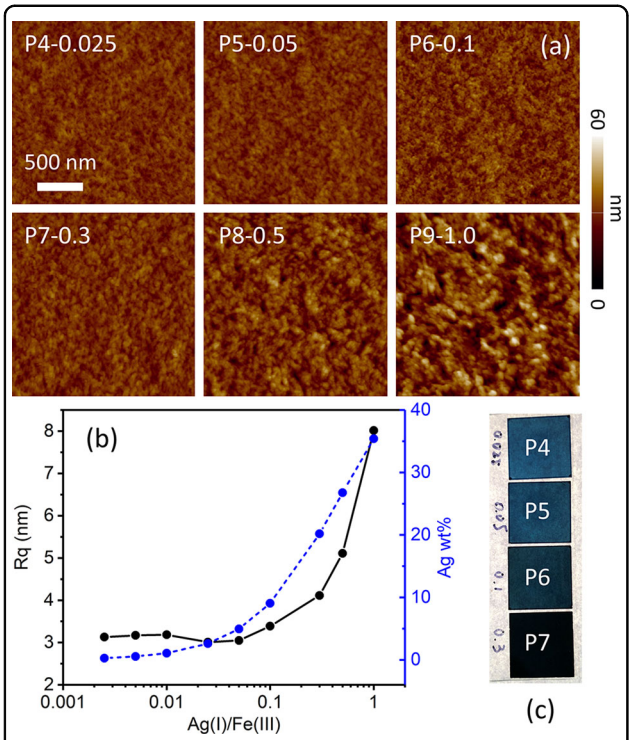

Fig. 3 Surface morphologies. a AFM images of nanocomposite films; **b** Surface roughness (R_q) as a function of Ag(I)/Fe(III) ratio; **c** Film appearances for samples P4 to P7.

pristine film (Fig. 4a, b). The existence of Ag QDs could increase σ to some extent, but this effect was overwhelmed by the negative influence of the high reaction rate. The lower the Ag wt% was, the farther σ was from the zero point at low temperatures. σ at the zero point was dominated by non-variable range hopping (VRH) conduction, which is affected by delocalization of carriers and is not temperature sensitive[6,10]. The relatively higher VRH conduction leads to a higher n toward 0 K. At higher temperatures, n can be further reduced by loading elemental Ag QDs. Especially for sample P1, the relatively lower n resulted in increased carrier mobility (Fig. 4c) compared with other samples. However, a similar enhancement was not observed for sample P3, which was also dominated by elemental Ag. Such a difference was likely caused by the thin Ag_2S layer formed on the surface of the particle (confirmed by the Raman spectrum), which altered the transportability of carriers. As a result, the average power factor of the film (Fig. 4d) reached a maximum of 63.1 μW/mK^2 at a Ag concentration of 0.2 wt%, and it could be maintained at a level of approximately 55 μW/mK^2 as long as the Ag concentration is below 0.5 wt %. The Seebeck coefficient was increased by nearly 20% at only 1.0 wt% Ag QD loading. Such enhancement was achieved without changing the oxidation status of the polymer, making the film much more stable in the atmosphere compared to reduced PEDOTs. To our surprise, the material outperformed the latest commercial PEDOT:PSS

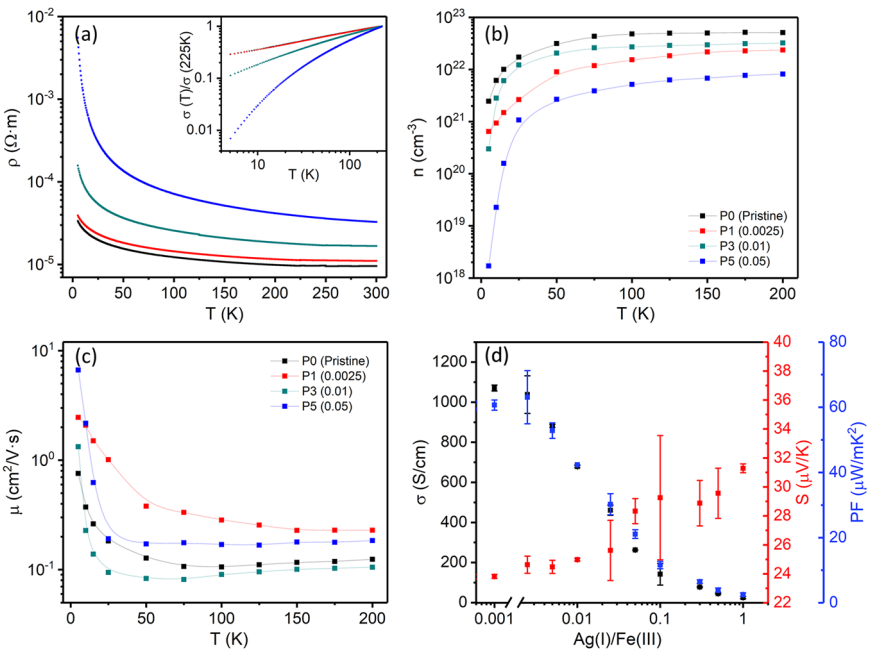

Fig. 4 Thermoelectric properties. a Temperature dependence of resistivities, **b** carrier concentrations, and **c** carrier mobilities for samples P0, P1, P3, and P5; **d** electrical conductivities, Seebeck coefficients and power factors (PF) of nanocomposite films.

Table 2 Comparison of this work with commercial PEDOT:PSS and other reported PEDOT-metal composites.

Material	(Additive or oxidant)/method	NPs wt%	σ (S/cm)	S (μV/K)	PF (μW/mK^2)	Ref.
Commercial PEDOT:PSS	Clevios PH1000 & 5 vol% DMSO	0	945	22.2	46.6	[10]
Porous PEDOT:Cl	$CuCl_2$/CVD	0	32	—	—	[35]
PEDOT:PSS/Au NPs	Dodecanethiol/Direct mixing	10^{-5} wt%	241	22	11.7	[37]
PEDOT:PSS/Au NPs	MHA[b]/Direct mixing	10^{-5} wt%	730	26.5	51.2	[38]
PEDOT:DBSA/Ag QD	**AgDBSA/VPP**	**0.2 wt%**	**1038**	**24.6**	**63.1**	**This work**
PEDOT:PSS/Ag nanowire	PVP[c]/Direct mixing	20 wt%	84.84	18.3	2.86	[39]
PEDOT:Cl/Cu NPs	$CuCl_2$/VPP	[a]	20	—	—	[36]
PEDOT: $(C_2F_5)_3PF_3$-Cu NPs	$CuCl_2$/Electropolymerization	[a]	2.5	—	—	[34]
PEDOT:Tos/Ag NPs	$AgNO_3$/Solution synthesis	[a]	6.49	14.2	0.13	[32]
$PEDOT_0$/Cu NPs	$Cu(NO_3)_2$/Solution synthesis	[a]	0.02	−2354	12.5	[32]
PEDOT:PSS/Au nanorod	PEG-thiol[d]/Direct mixing	75 wt%	~2000	~12	~28.8	[40]

[a]Determined by the stoichiometric ratio (usually above 20 wt%).
[b]6-mercaptohexanoic acid.
[c]poly-(N-vinyl-2-pyrrolidone).
[d]Poly(ethylene glycol) methyl ether thiol.

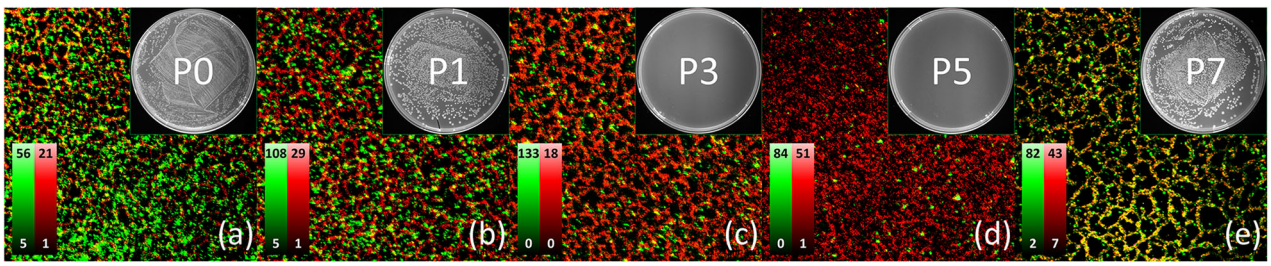

Fig. 5 Antibacterial activities. Samples (**a**) P0, (**b**) P1, (**c**) P3, (**d**) P5 and (**e**) P7 were examined with both microimaging and live/dead strain methods. Red area: dead cells. Green area: live cells.

product (Clevios PH1000)[10] and almost all previously reported PEDOT-metal composite materials[34–40], as summarized in Table 2.

The antibacterial activities of the samples (Fig. 5) are determined by the Ag QDs existing in the film. Ag_2S QDs contribute much less antibacterial ability than elemental Ag QDs. According to the live/dead results and the corresponding micro images, the bacterial killing effect coincided well with the actual elemental Ag wt%.

Conclusion

We successfully synthesized micron-thick S-PEDOT-Ag QD composite films through a one-step surfactant-free VPP approach using a novel multifunctional Ag(I) oxidant. The TE performance was optimized by effective thermal power enhancement at low Ag concentrations. The antibacterial effect as well as some unique characteristics of composite films may also find utility in applications such as wearable electric devices or sensors. Extensive studies on nonferric oxidants as well as on the VPP process itself are needed for the future development of high-performance S-PEDOT composites.

Acknowledgements
This research was funded by the National Natural Science Foundation of China (Nos. 21905293, 52072391 and 91963208) and Shanghai Municipal Natural Science Foundation (21ZR1473200).

Author details
[1]State Key Laboratory of High Performance Ceramics and Superfine Microstructure, Shanghai Institute of Ceramics, Chinese Academy of Sciences, Shanghai, China. [2]Department of Materials Science and Engineering, Yonsei University, Seoul, South Korea. [3]School of Materials Science and Engineering, Hebei University of Technology, Tianjin, China

Author contributions
W.S. synthesized the films and wrote the draft. S.Q. and Q.Y. supervised the work and revised the paper. W.D. characterized the antibacterial activities. Y.C. obtained the XRD data and measured the film thickness. K.H.L. arranged NMR and LC–MS characterizations and revised the paper. L.C. initiated the work and led the project.

Conflict of interest
The authors declare no competing interests.

Publisher's note
Springer Nature remains neutral with regard to jurisdictional claims in published maps and institutional affiliations.

Supplementary information The online version contains supplementary material available at https://doi.org/10.1038/s41427-022-00391-7.

Received: 29 November 2021 Revised: 3 March 2022 Accepted: 13 April 2022.
Published online: 3 June 2022

References

1. Du, Y., Shen, S. Z., Cai, K. & Casey, P. S. Research progress on polymer–inorganic thermoelectric nanocomposite materials. *Prog. Polym. Sci.* **37**, 820–841 (2012).
2. Saranya, K., Rameez, M. & Subramania, A. Developments in conducting polymer based counter electrodes for dye-sensitized solar cells: an overview. *Eur. Polym. J.* **66**, 207–227 (2015).
3. Zhao, Z. et al. PEDOT-based composites as electrode materials for supercapacitors. *Nanotechnology* **27**, 042001 (2016).
4. Hui, Y., Bian, C., Xia, S., Tong, J. & Wang, J. Synthesis and electrochemical sensing application of poly(3,4-ethylenedioxythiophene)-based materials: a review. *Anal. Chim. Acta* **1022**, 1–19 (2018).
5. Bharti, M., Singh, A., Samanta, S. & Aswal, D. K. Conductive polymers for thermoelectric power generation. *Prog. Mater. Sci.* **93**, 270–310 (2018).
6. Shi, W. et al. Ch. 4, 69–96 (Springer, Cham, Switzerland, 2019).
7. Elschner, A., Kirchmeyer, S., Lövenich, W., Merker, U., Reuter, K., *PEDOT: Principles and Applications of an Intrinsically Conductive Polymer*. (Taylor & Francis Group, NW, USA, 2011).
8. Bubnova, O. et al. Semi-metallic polymers. *Nat. Mater.* **13**, 190–194 (2014).
9. Bae, E. J., Kang, Y. H., Jang, K. S., Lee, C. & Cho, S. Y. Solution synthesis of telluride-based nano-barbell structures coated with PEDOT:PSS for spray-printed thermoelectric generators. *Nanoscale* **8**, 10885–10890 (2016).
10. Zhang, B., Sun, J., Katz, H. E., Fang, F. & Opila, R. L. Promising thermoelectric properties of commercial PEDOT:PSS materials and their Bi2Te3 powder composites. *ACS Appl. Mater. Interfaces* **2**, 3170–3178 (2010).
11. See, K. C. et al. Water-processable polymer-nanocrystal hybrids for thermoelectrics. *Nano Lett.* **10**, 4664–4667 (2010).
12. Gueye, M. N. et al. Structure and dopant engineering in PEDOT thin films: practical tools for a dramatic conductivity enhancement. *Chem. Mater.* **28**, 3462–3468 (2016).
13. Aasmundtveit, K. E. et al. Structure of thin films of poly(3,4-ethylenedioxythiophene). *Synth. Met.* **101**, 561–564 (1999).
14. Evans, D. et al. Structure-directed growth of high conductivity PEDOT from liquid-like oxidant layers during vacuum vapor phase polymerization. *J. Mater. Chem.* **22**, 14889–14895 (2012).
15. Mueller, M. et al. Vacuum vapour phase polymerization of high conductivity PEDOT: Role of PEG-PPG-PEG, the origin of water, and choice of oxidant. *Polymer* **53**, 2146–2151 (2012).
16. Massonnet, N., Carella, A., de Geyer, A., Faure-Vincent, J. & Simonato, J. P. Metallic behaviour of acid doped highly conductive polymers. *Chem. Sci.* **6**, 412–417 (2015).
17. Bubnova, O. et al. Optimization of the thermoelectric figure of merit in the conducting polymer poly(3,4-ethylenedioxythiophene). *Nat. Mater.* **10**, 429–433 (2011).
18. Wang, J., Cai, K. & Shen, S. A facile chemical reduction approach for effectively tuning thermoelectric properties of PEDOT films. *Org. Electron.* **17**, 151–158 (2015).
19. Wang, J., Cai, K. & Shen, S. Enhanced thermoelectric properties of poly(3,4-ethylenedioxythiophene) thin films treated with H_2SO_4. *Org. Electron.* **15**, 3087–3095 (2014).
20. Yi, C. et al. Highly electrically conductive polyethylenedioxythiophene thin films for thermoelectric applications. *J. Mater. Chem. A.* **4**, 12730–12738 (2016).
21. Winther-Jensen, B., Breiby, D. W. & West, K. Base inhibited oxidative polymerization of 3,4-ethylenedioxythiophene with iron(III)tosylate. *Synth. Met.* **152**, 1–4 (2005).
22. Fabretto, M., Zuber, K., Hall, C., Murphy, P., Griesser, H. J. The role of water in the synthesis and performance of vapour phase polymerised PEDOT electrochromic devices. *J. Mater. Chem.* ***19*** (2009).
23. Kim, J., Kim, E., Won, Y., Lee, H. & Suh, K. The preparation and characteristics of conductive poly(3,4-ethylenedioxythiophene) thin film by vapor-phase polymerization. *Synth. Met.* **139**, 485–489 (2003).
24. Levermore, P. A., Chen, L., Wang, X., Das, R. & Bradley, D. D. C. Fabrication of highly conductive Poly(3,4-ethylenedioxythiophene) films by vapor phase polymerization and their application in efficient organic light-emitting diodes. *Adv. Mater.* **19**, 2379–2385 (2007).
25. Park, T., Park, C., Kim, B., Shin, H., Kim, E. Flexible PEDOT electrodes with large thermoelectric power factors to generate electricity by the touch of fingertips. *Energy Environ. Sci.* ***6*** (2013).
26. Fabretto, M., Muller, M., Zuber, K. & Murphy, P. Influence of PEG-ran-PPG surfactant on vapour phase polymerised PEDOT thin films. *Macromol. Rapid Commun.* **30**, 1846–1851 (2009).
27. Kirchmeyer, S., Freidrich, J. US patent 20030161941A1 (2003).
28. Shi, W. et al. Micron-thick highly conductive PEDOT films synthesized via self-inhibited polymerization: roles of anions. *NPG Asia Mater.* **9**, e405–e405 (2017).
29. Culebras, M., Gómez, C. M. & Cantarero, A. Enhanced thermoelectric performance of PEDOT with different counter-ions optimized by chemical reduction. *J. Mater. Chem. A.* **2**, 10109–10115 (2014).
30. Shi, W. et al. One-step synthesis and enhanced thermoelectric properties of polymer-quantum dot composite films. *Angew. Chem. Int. Ed.* **57**, 8037–8042 (2018).
31. Corradi, R. & Armes, S. P. Chemical synthesis of poly(3,4-ethylenedioxythiophene). *Synth. Met.* **84**, 453–454 (1997).
32. Wang, Y., Cai, K., Chen, S., Shen, S. & Yao, X. One-step interfacial synthesis and thermoelectric properties of Ag/Cu-poly(3,4-ethylenedioxythiophene) nanostructured composites. *J. Nanopart. Res.* **16**, 2531 (2014).
33. Kumar, S. S., Kumar, C. S., Mathiyarasu, J. & Phani, K. L. Stabilized gold nanoparticles by reduction using 3,4-Ethylenedioxythiophene-polystyrenesulfonate in aqueous solutions: nanocomposite formation, stability, and application in catalysis. *Langmuir* **23**, 3401–3408 (2007).
34. Reddy, B. N., Pathania, A., Rana, S., Srivastava, A. K. & Deepa, M. Plasmonic and conductive Cu fibers in poly (3,4-ethylenedioxythiophene)/Cu hybrid films: Enhanced electroactivity and electrochromism. *Sol. Energ. Mat. Sol. C.* **121**, 69–79 (2014).
35. Im, S. G. et al. Conformal coverage of Poly(3,4ethylenedioxythiophene) films with tunable nanoporosity via oxidative chemical vapor deposition. *ACS Nano.* **2**, 1959–1967 (2008).
36. Cho, M. S., Kim, S. Y., Nam, J. D. & Lee, Y. Preparation of PEDOT/Cu composite film by in situ redox reaction between EDOT and copper(II) chloride. *Synth. Met.* **158**, 865–869 (2008).
37. Toshima, N., Jiravanichanun, N. & Marutani, H. Organic thermoelectric materials composed of conducting polymers and metal nanoparticles. *J. Electron. Mater.* **41**, 1735–1742 (2012).
38. Toshima, N. & Jiravanichanun, N. Improvement of thermoelectric properties of PEDOT/PSS films by addition of gold nanoparticles: enhancement of seebeck coefficient. *J. Electron. Mater.* **42**, 1882–1887 (2013).
39. Liu, Y. et al. Preparation of bulk AgNWs/PEDOT:PSS composites: a new model towards high-performance bulk organic thermoelectric materials. *RSC Adv.* **5**, 45106–45112 (2015).
40. Yoshida, A. & Toshima, N. Gold nanoparticle and gold nanorod embedded PEDOT:PSS thin films as organic thermoelectric materials. *J. Electron. Mater.* **43**, 1492–1497 (2013).